Paper 168

COMPUTATIONAL ASSESSMENT OF FLOW BREAKDOWN IN CLOSED SECTION MODEL ROTOR TESTS

M. Biava[1], A. Thomopoulos[2], L. Vigevano[3]

[1] AgustaWestland-Politecnico Advanced Rotorcraft Center, Milano, Italy,
e-mail: biava.awparc@agustawestland.com
[2] AgustaWestland S.p.A., Cascina Costa di Samarate (VA), Italy
[3] Dipartimento di Ingegneria Aerospaziale - Politecnico di Milano, Milano, Italy

Abstract

A qualitative analysis of the flow inside the closed test section of the Politecnico di Milano large wind tunnel in presence of rotor effects has been carried out with the *ROSITA* RANS solver. The rotor is represented as an actuator disk. The analysis of the results of the performed steady state simulations allow for the determination of the flow breakdown boundaries in terms of tunnel operating parameters. Some indications are provided on experimental measurements which may be used for an on-line detection of the flow breakdown itself.

1 Introduction

Notwithstanding the increasing capability of CFD methods in predicting rotor performances, the use of wind tunnel test measurements will continue to play a key role in the development of new rotor systems. The question is open, however, on how to operate the model rotor within the wind tunnel so as to reproduce free air conditions. In fact, accurate measurements of rotor performance as achieved in a wind tunnel are strongly influenced by the test section configuration, whether it be closed or open jet. In particular, rotor tests at low speed and high thrust in a closed test section tunnel may experience what is known as *flow breakdown*, that happens when the interaction between the rotor wake and the tunnel walls strongly modify the flow in the vicinity of the rotor due to the onset of recirculation phenomena [1]. In flow breakdown condition the wind tunnel environment is no more representative of the free air environment and the rotor performance cannot be adjusted by means of wall corrections. Such operating conditions are clearly to be avoided in a test programme.

Shinoda [2] addressed the study of wall interference effects and the identification of flow breakdown by means of an extensive experimental campaign in the 80×120 foot wind tunnel at NASA Ames. The present research is instead based on purely numerical techniques, with the objective of defining the flow breakdown envelope for the 4×3.8 m closed test section of the Politecnico di Milano (PoliMi) large wind tunnel, and also of investigating which experimental indicators may be utilized to recognize the flow breakdown condition during model rotor tests. To this end, a campaign of numerical simulations has been carried out to characterize the flow field in the closed test section generated by the AgustaWestland AW139 model rotor. The computations were performed with the CFD code ROSITA (ROtorcraft Software ITAly) based on the solution of the Reynolds Averaged Navier-Stokes equations coupled with the one-equation turbulence model of Spalart-Allmaras. The rotor effect is represented with an actuator disk model. The numerical solutions were run for several values of the rotor thrust and of the advance ratio. Visualizations of the computed flow field are used to detect the onset of flow breakdown.

2 The flow solver ROSITA

The *ROSITA* CFD solver has been developed at the Aerospace Department of PoliMi over the last ten years, and is currently used and continuously improved at AWPARC and at AgustaWestland. It solves the Euler, Navier-Stokes and Reynolds Averaged Navier-Stokes (RANS) equations in overset systems of moving multi-block grids. The equations are discretized in space by means of a cell-centred finite-volume implementation of the Roe's scheme [3]. Second order accuracy is obtained through the use of MUSCL extrapolation supplemented with a modified version of the Van Albada limiter proposed by Venkatakrishnan [4]. The viscous terms are computed using either a cell-centred discretization scheme, the Swanson and Turkel scheme or the Martinelli scheme. Time advancement is carried out with a dual-time formulation [5]. A 2^{nd} order backward differentiation formula is applied to approximate the time derivative and a fully unfactored implicit scheme is used in pseudo-time. The generalized conjugate gradient (GCG) method is used to solve the resulting linear system, with preconditioning based on a block incomplete lower-upper (BILU) factorization. The RANS equations can be coupled with the simple algebraic models of Michel and Baldwin-Lomax or with the one-equation turbulence model of Spalart-Allmaras.

The connectivity between the component grids is computed by means of the well known Chimera technique. The approach adopted in *ROSITA* is derived from that originally proposed by Chesshire and Henshaw [6]: the domain boundaries with solid wall conditions are firstly identified and all points in overlapping grids that fall close to these boundaries are marked as holes (seed points). Then, an iterative algorithm identifies the donor and fringe points and lets the hole points grow from the seeds until they fill entirely the regions outside the computational domain. To speed up the search of donor points, oct-tree and ADT (alternating digital tree) data structures are employed.

The *ROSITA* solver is fully capable of running in parallel on computing clusters. The parallel algorithm is based on the message passing programming paradigm and the parallelization strategy consists in distributing the grid blocks among the available processors. Each grid block can be automatically subdivided into smaller blocks by the CFD solver to attain an optimal load balancing.

3 Numerical model and test cases

Figure 1 shows the domain used for the simulations of the closed test section of the PoliMi large wind tunnel. The grid system consists of a cylindrical mesh, containing the actuator disk representing the AW139 model rotor, and of a background cartesian mesh, modelling the closed test section of the wind tunnel. The actuator disk is placed at a distance $h = 1.9\,\mathrm{m}$ from the floor, that is, in terms of the rotor radius, $h/R = 2.14$, being $R = 0.8875\,\mathrm{m}$. A parameter that is commonly used to correlate the operating conditions to the wall interference effects is the ratio between the rotor diameter and the width w of the wind tunnel test section; for the present case we have $2R/w = 0.44$.

The solution is exchanged between the two grids thanks to the Chimera technique. In total the mesh counts about 2.4 million cells. The background mesh has been created with *ANSYS ICEMCFD*, while the cylindrical mesh has been created with the in-house code *backCYL*. The applied boundary conditions are:

- inviscid wall boundary conditions on the wind tunnel walls;
- velocity inlet at the inflow boundary;
- pressure outlet at the outflow boundary.

The actuator disk is seen as a distribution of linear momentum sources over a disk-shaped grid plane of the cylindrical grid. The distribution of the source strength has been derived by previous full-rotor forward flight CFD simulations. As can be noticed by figure 1, the actuator disk has been positioned

parallel to the wind tunnel floor. This is consistent, since the forward flight simulations that provided the actuator disk load distributions were performed placing the mast in vertical direction and trimming the rotor to have zero sine and cosine harmonic components for the flapping motion, so as to have a tip path plane parallel to the floor. Furthermore, the selected configuration can be considered as one which maximize the interference effects between rotor wake and tunnel walls. It is also frequently used in model rotor experimental tests, although may not be the correct one to represent free flight conditions.

With respect to the real geometry, the test section grid has the correct dimensions in the cross sections normal to the tunnel axis (4×3.8m), but has a higher length. Indeed, its length is 16m instead of the actual 4m of the real test section. This is done to move the inflow and outflow boundaries away from the actuator disk, so as to reduce the undesired reflection of perturbations inside the flow domain associated to the numerical treatment of the boundary conditions.

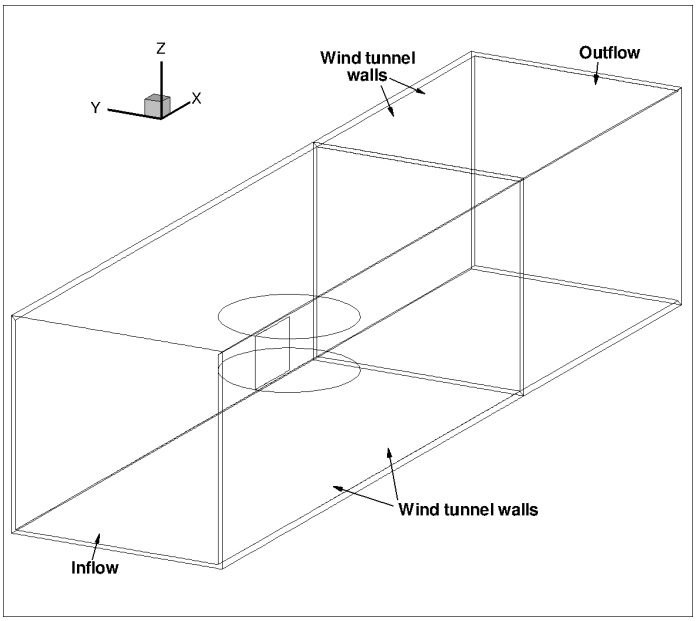

Figure 1: Boundaries of the closed test section computational grid.

The numerical simulations cover the advance ratio interval $0.02 < \mu < 0.21$ for three different value of the thrust coefficient $C_T/\sigma = 0.08 - 0.10 - 0.12$. The steady simulations have been performed with the RANS solver using the Spalart-Allmaras turbulence model. The solver was run in parallel on 16 processors so that each test case took about 20 to 40 hours to complete, depending upon the number of iterations needed to attain convergence.

4 Analysis of results

All the selected wind tunnel and rotor conditions were simulated with the assumption of a steady flow. During the analysis of the numerical results it turned out that not in all the considered conditions the flow parameters were compatible with a steady flow. In fact, if we look at figure 2, which shows the force normal to the wind tunnel floor for the advance ratio $\mu = 0.023$, we notice that the load oscillations are never completely damped out and the solution does not attain a converged steady state. The same happens, to a lesser degree, for advance ratios up to $\mu = 0.047$ (cfr. figure 3). The explanation relies on the fact that at this low operating speed the rotor wake impinges on the wind tunnel floor and tends to be convected upstream, generating complex (intrinsically unsteady) vortical structures possibly interacting with the rotor itself, as can be observed in figures 4–5 showing the y-component

of the vorticity vector in the vertical symmetry plane of the wind tunnel for $\mu = 0.023 - 0.047$.

Nevertheless, the (forcedly) steady solutions were retained as a good reference to understand the overall qualitative pattern of the flow inside the wind tunnel test section also at the lower speeds. This is justified in view of the fact that the main objective of the present analysis is to define the boundary of the flow breakdown region. Clearly, the solutions attaining a steady state are characterized by a low level of interaction between the wake and the tunnel walls and are probably representative of free air conditions. *Vice versa*, the solutions that cannot reach the steady state probably fall in the flow breakdown region, since the unsteadiness is likely to be a symptom of the onset of flow recirculations.

For advance ratios $\mu \geq 0.070$ the simulations seem to reach a reasonably convergent state (see figures 6 and 7). For these higher speeds, in fact, there is little or no interaction between the wake and the tunnel walls as can be seen in figures 8–9, and the flow is thus steady.

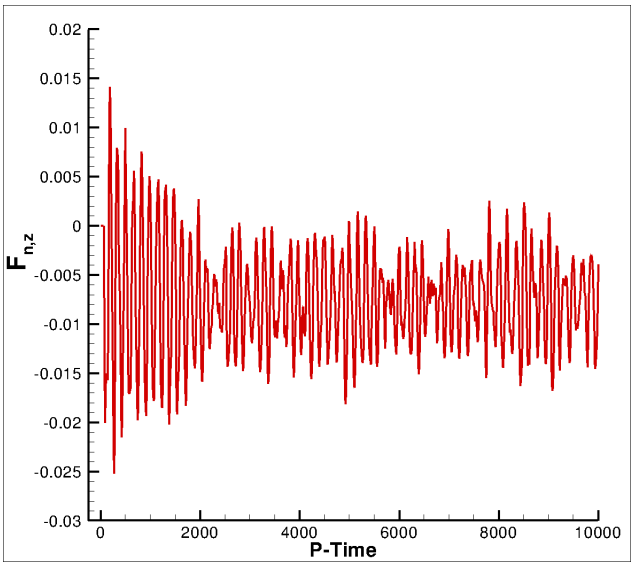

Figure 2: Force convergence of the simulations for $\mu = 0.023$ and $C_T/\sigma = 0.1$.

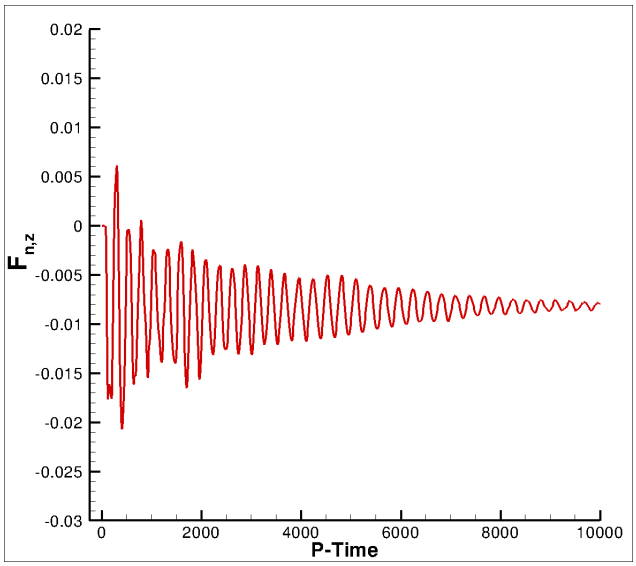

Figure 3: Force convergence of the simulations for $\mu = 0.047$ and $C_T/\sigma = 0.1$.

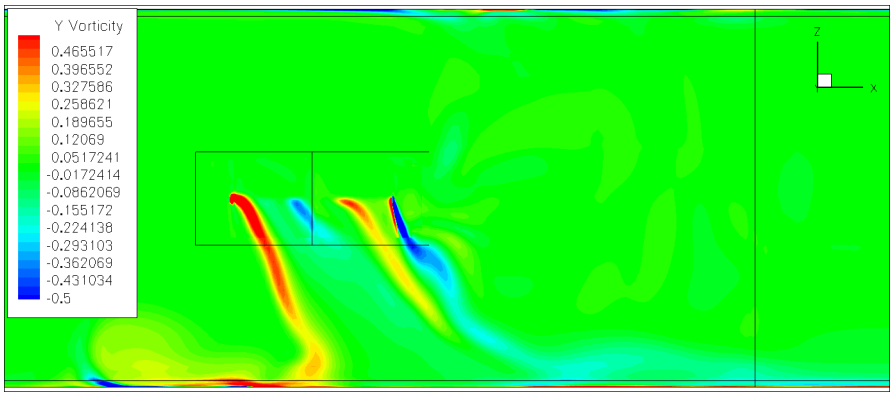

Figure 4: Y-Vorticity in plane $y = 0$ for $\mu = 0.023$ and $C_T/\sigma = 0.1$.

Figures 10 to 13 show the local flow Mach number in the cross-flow plane corresponding to the rotor hub and in the symmetry plane of the tunnel, plotted together with the velocity field streamtraces at some selected advance ratios in the range $0.023 < \mu < 0.094$ and with fixed $C_T/\sigma = 0.1$.

At $\mu = 0.023$ the pattern of the flow is very complex: the wake of the rotor impinges on the wind tunnel floor right below the rotor itself, then partly moves upstream and generates complex vortical

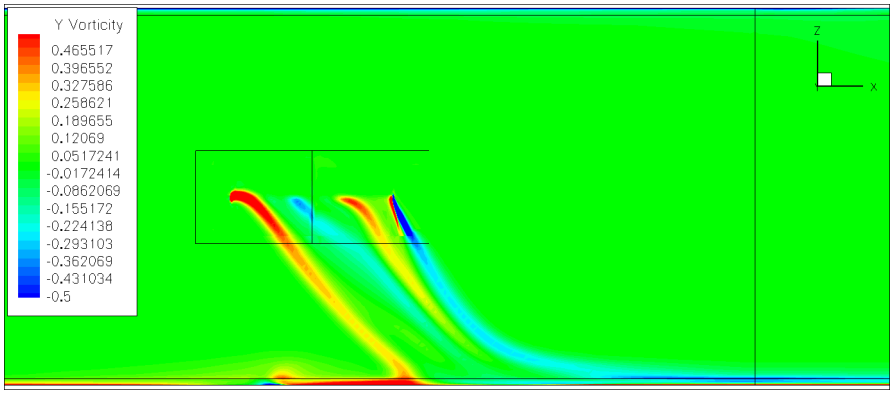

Figure 5: Y-Vorticity in plane $y = 0$ for $\mu = 0.047$ and $C_T/\sigma = 0.1$.

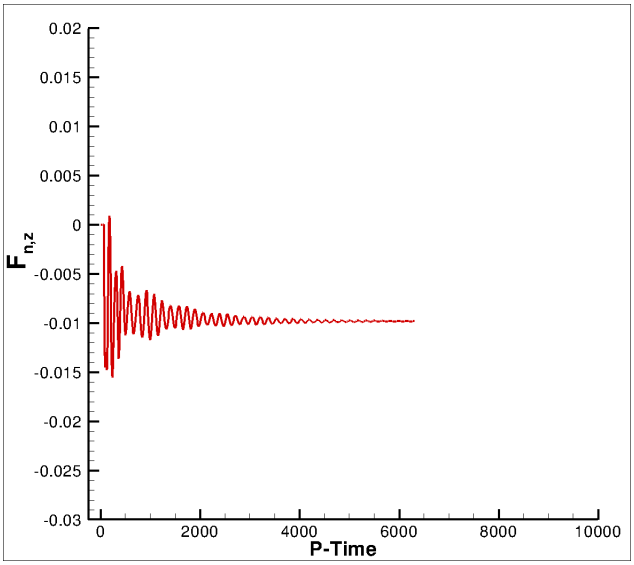

Figure 6: Force convergence of the simulations for $\mu = 0.070$ and $C_T/\sigma = 0.1$.

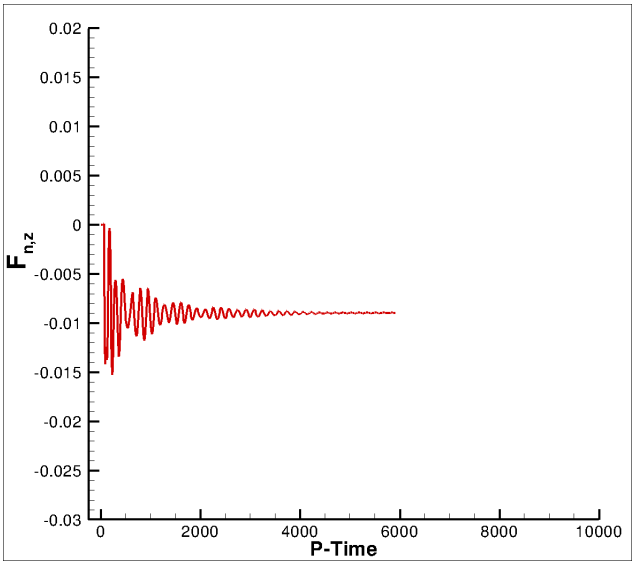

Figure 7: Force convergence of the simulations for $\mu = 0.094$ and $C_T/\sigma = 0.1$.

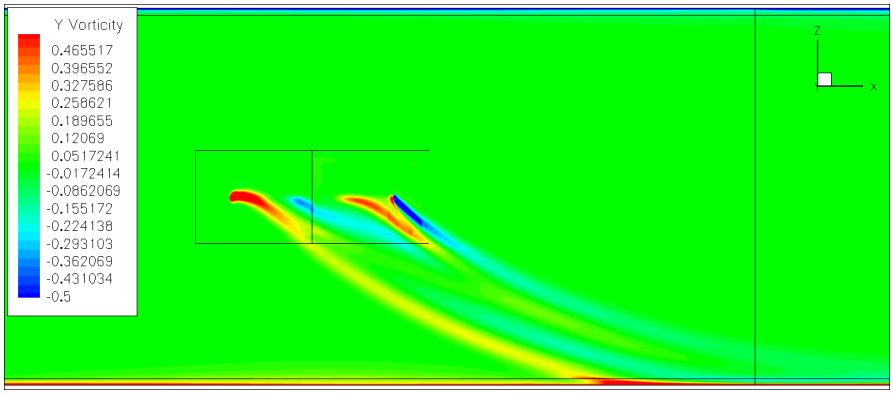

Figure 8: Y-Vorticity in plane $y = 0$ for $\mu = 0.070$ and $C_T/\sigma = 0.1$.

structures with irregular spatial distribution (see figure 10). At this wind tunnel speed, and for all the considered values of the thrust coefficient $C_T/\sigma = 0.08$–0.12, the wind tunnel test is not recommended, due to the strong rotor-wake interaction induced by the wind tunnel walls.

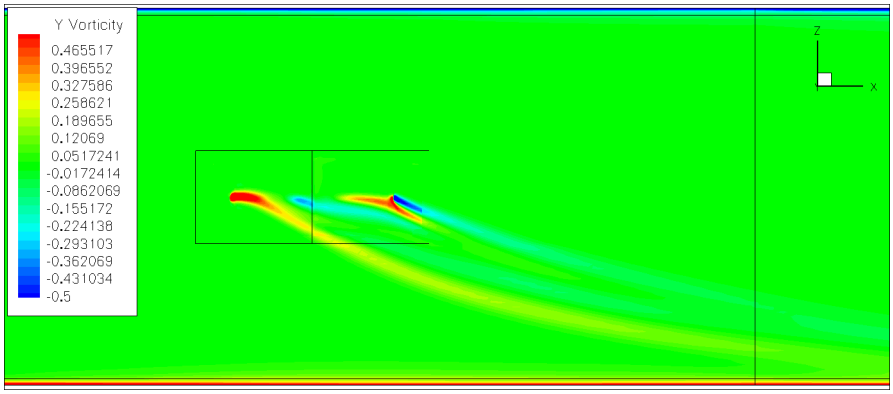

Figure 9: Y-Vorticity in plane $y = 0$ for $\mu = 0.094$ and $C_T/\sigma = 0.1$.

When the advance ratio is raised to 0.047 the flow exhibits a more regular behavior, with the formation of a clearly distinguishable horseshoe vortex close to the test section floor, in front and below the rotor (see figure 11). In this intermediate situation the rotor self-interaction is lower with respect to the $\mu = 0.023$ case, but the deflection of the wake by the tunnel walls is still very strong. This fact and the presence of the horseshoe vortex close to the rotor, make testing in these operating conditions not recommended or, at least, worth for further investigations.

For advance ratios of 0.070 and higher the situation improves significantly (see figures 12–13). At $\mu = 0.070$ the wake impinges on the floor at more than one rotor diameter behind the model, and for $\mu > 0.094$ there's no more visible strong interaction between the wake and the wind tunnel floor and side walls for at least three rotor diameters. This seems to be compatible with rotor testing and the acquisition of reliable performance data.

To sum up, after the analysis of the flow inside the wind tunnel test section for several wind tunnel speeds and rotor thrust coefficients, the following recommendations can be given:

- regardless of the value of the thrust coefficient in the considered range ($C_T/\sigma = 0.08$–0.12), the wind tunnel environment for advance ratios higher than 0.070 is representative of free air conditions;
- for advance ratios below 0.047 the rotor is strongly interacting with its own wake and therefore its performance cannot be corrected to free air by means of a wall correction procedure;
- the advance ratios in the range $0.047 - 0.070$ represent a transition regime in which the flow breakdown appears, and it is difficult (only on the basis of the previous analysis) to tell to what degree the performance measurements can be related to the free air conditions.

5 Flow breakdown identification

The analysis of the previous section identified the operating conditions at which flow breakdown occurs in the closed test section of the large wind tunnel of PoliMi. On the basis of the same numerical results, it is possible to give some guidelines on how to detect the flow breakdown during actual wind tunnel tests by monitoring some easily measurable quantities.

Figures 14 to 18 present the pressure distribution on the wind tunnel floor for advance ratios between 0.023 and 0.094. On the same figures, the streamtraces of the surface shear stress vector field are also plotted.

The analysis of these figures suggests two possible ways for identifying the occurrence of flow breakdown. The first one is by measuring the static pressure at some selected points on the centerline

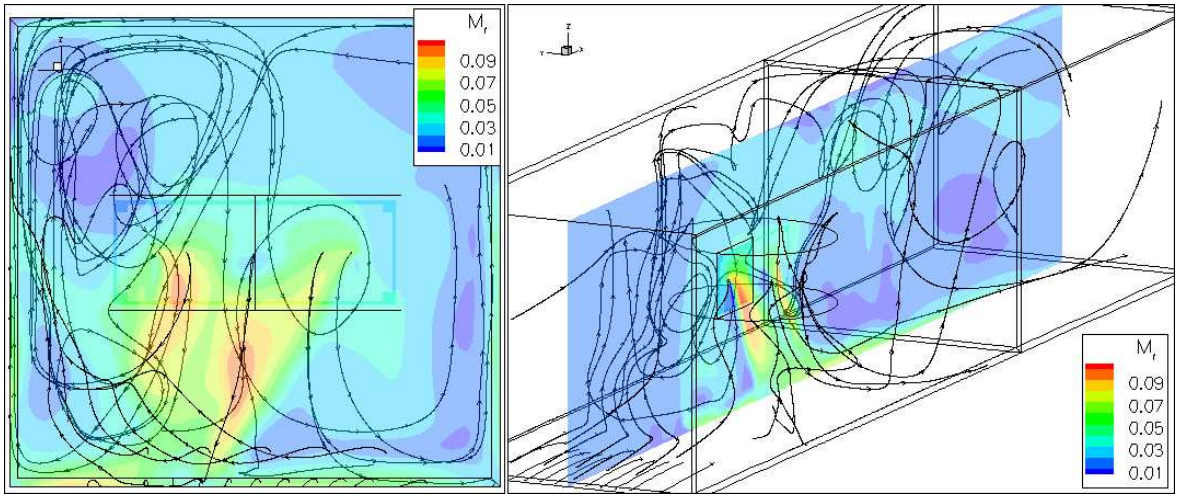

Figure 10: Flow in the closed test section for $\mu = 0.023$ and $C_T/\sigma = 0.1$.

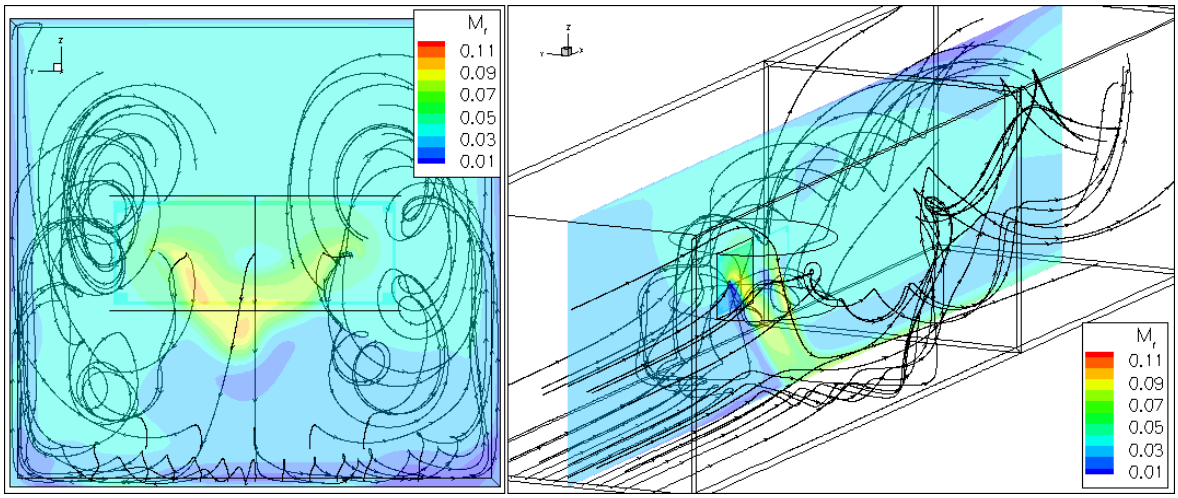

Figure 11: Flow in the closed test section for $\mu = 0.047$ and $C_T/\sigma = 0.1$.

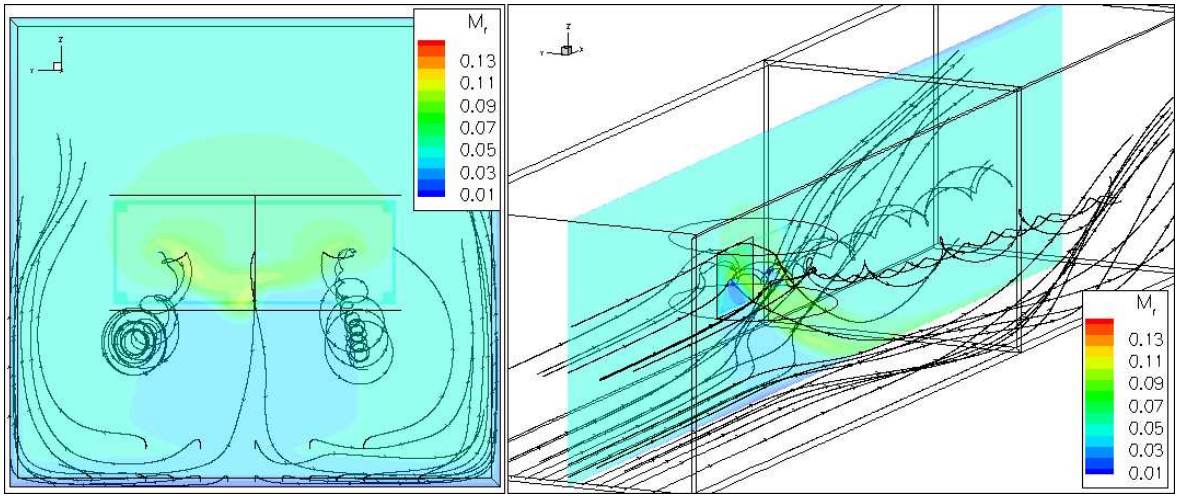

Figure 12: Flow in the closed test section for $\mu = 0.070$ and $C_T/\sigma = 0.1$.

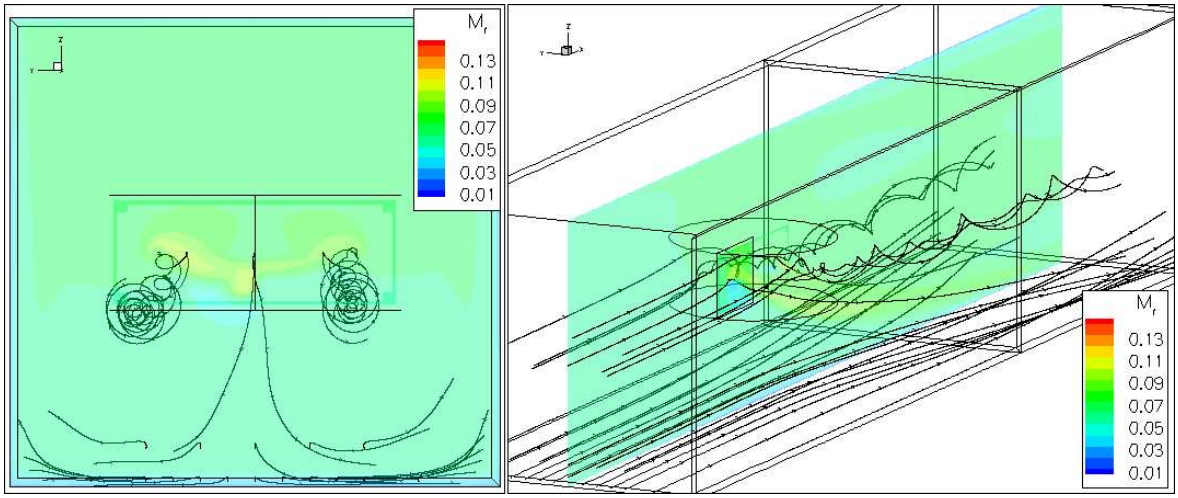

Figure 13: Flow in the closed test section for $\mu = 0.094$ and $C_T/\sigma = 0.1$.

of the wind tunnel floor, starting from one diameter in front of the rotor model and down to half/one diameter behind. In fact, it can be noticed that when the downwash impinges on the floor it induces a local raise of the static pressure about the floor centerline. The position of this high pressure spot can in turn be easily related to the flow speed and thus to the onset of the flow breakdown.

However, the measurement of the static pressure could require the drilling of holes on the wind tunnel floor, which may be undesirable. The second, less invasive, option suggested by figures 14–18 for identifying the presence of flow breakdown is to monitor the shear stress field on the tunnel floor. This can be easily done for instance by sticking lines of wool-tufts on the wind tunnel floor at selected stations in the flow direction, starting from a distance of two diameters ahead of the rotor model and down to half diameter behind.

By inspection of the figures, we deduce that for advance ratios higher than 0.094 all the tufts should direct themselves roughly parallel to the tunnel axis and symmetrically with respect to the vertical symmetry plane of the test section. Additionally, their movements should be very limited to denote the presence of a steady flow.

For advance ratios below 0.047, on the other hand, some or all the tufts lines should exhibit a very unsteady movement and the average direction of front lines should be pointing upstream, to reflect the presence of the vortical structures generated by the impingement of the wake on the floor and its upstream motion. Also these flow regimes could therefore be easily detected.

The cases $0.059 < \mu < 0.070$ are in the transition regime and should be characterized by a medium level of unsteadiness of the tufts. Moreover the front lines of tufts should be pointing upstream while the lines below the rotor should be pointing sidewards.

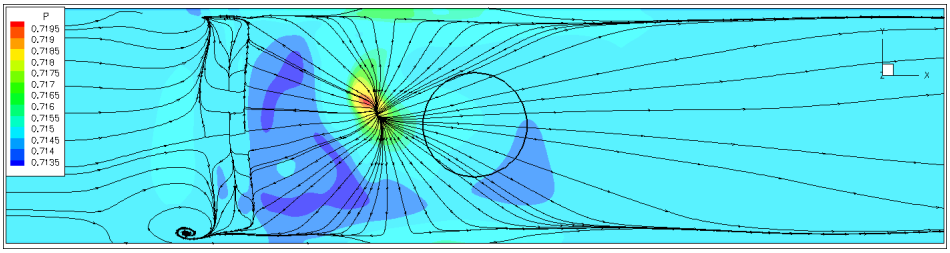

Figure 14: Pressure distribution and streamtraces of the shear stress vector field on the floor for $\mu = 0.023$ and $C_T/\sigma = 0.1$.

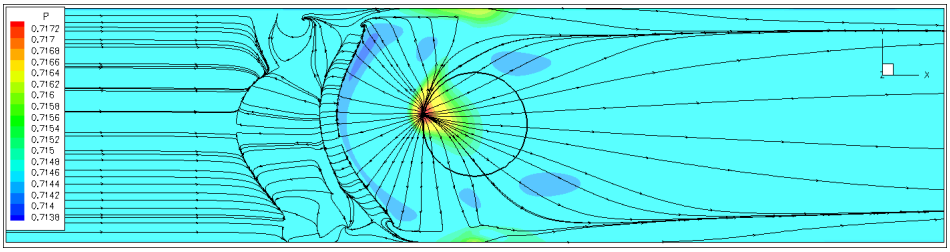

Figure 15: Pressure distribution and streamtraces of the shear stress vector field on the floor for $\mu = 0.047$ and $C_T/\sigma = 0.1$.

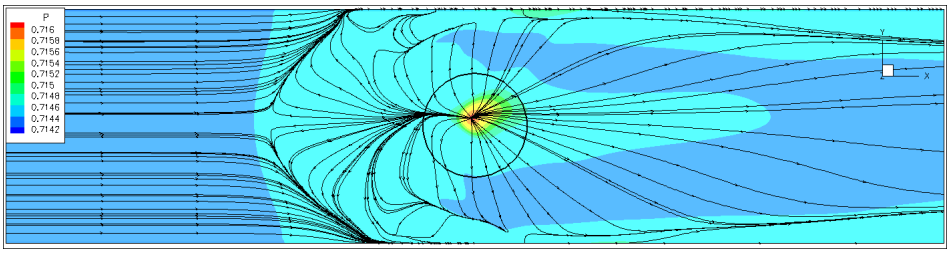

Figure 16: Pressure distribution and streamtraces of the shear stress vector field on the floor for $\mu = 0.059$ and $C_T/\sigma = 0.1$.

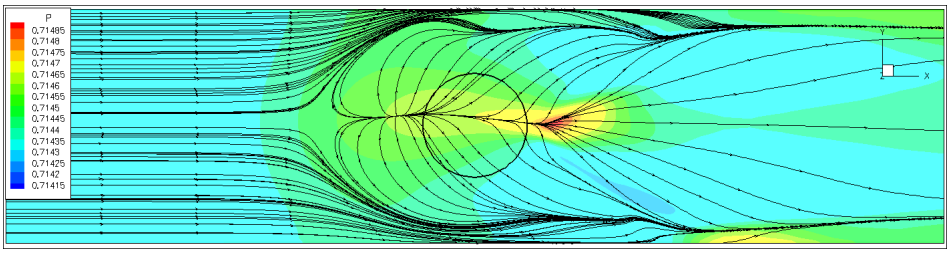

Figure 17: Pressure distribution and streamtraces of the shear stress vector field on the floor for $\mu = 0.070$ and $C_T/\sigma = 0.1$.

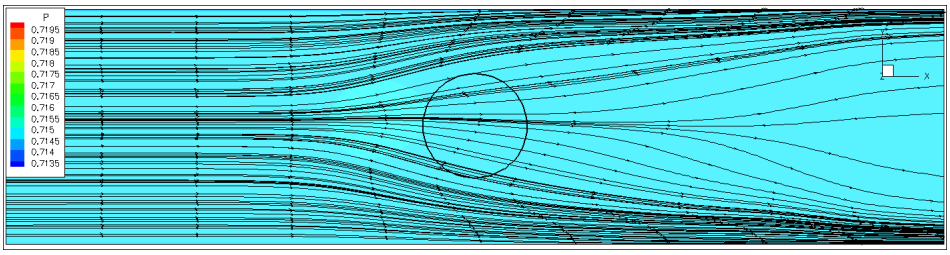

Figure 18: Pressure distribution and streamtraces of the shear stress vector field on the floor for $\mu = 0.094$ and $C_T/\sigma = 0.1$.

6 Conclusions

The paper reports the qualitative analysis of the flow inside the closed test section of PoliMi large wind tunnel in the presence of rotor effects. The flow has been simulated with the flow solver *ROSITA*, adopting an actuator disk model of the AW139 rotor to account for the rotor effects in the numerical solution. The load distributions for the development of the actuator disk model were extracted from previous forward flight simulations.

The CFD solutions have been analyzed in order to define the operating parameter range, in terms of wind tunnel speed and rotor thrust, in correspondence of which the flow is qualitatively similar to that of the free air conditions, so that the measured rotor performance can be corrected to account for the wall interference. The boundary of the region of these allowed operating parameters corresponds to the occurrence of the flow breakdown, which happens when the interaction between the rotor wake and the wind tunnel walls generates recirculation of the flow in proximity of the rotor. In the PoliMi wind tunnel closed test section, flow breakdown may be avoided, for a rotor load range with $C_T/\sigma \leq 0.12$, selecting advance ratio values larger than 0.07. Moreover, some indications have been given on how to detect on-line the occurrence of flow breakdown during the actual wind tunnel tests by monitoring easily measurable quantities.

Acknowledgements The present work has been carried out within the WITCH project, funded by AWPARC.

References

[1] J.-J. Philippe. Consideration on wind-tunnel testing techniques for rotorcrafts. In *AGARD Special Course on Aerodynamics of Rotorcraft*, 1990.

[2] P. M. Shinoda. Wall interaction effects for a full-scale helicopter rotor in the NASA Ames 80- by 120-foot wind tunnel. In *AGARD Meeting on "Wall Intereference, Support Interference and Flow Field Measurements"*, 1993.

[3] P.L. Roe. Approximate riemann solvers, parameter vectors and difference schemes. *Journal of Computational Physics*, 43:357–372, 1981.

[4] V. Venkatakrishnan. On the accuracy of limiters and convergence to steady state solutions. 31^{st} *AIAA Aerospace Sciences Meeting and Exhibit*, AIAA 93-0880, 1993. Reno, Nevada.

[5] A. Jameson. Time dependent calculations using multigrid with applications to unsteady flows past airfoils and wings. 10^{th} AIAA Computational Fluid Dynamics Conference, Honolulu, HI, AIAA 91-1596.

[6] G. Chesshire and W. D. Henshaw. Composite overlapping meshes for the solution of partial differential equations. *J. Comp. Phys.*, 90:1–64, 1990.